Magn Reson Med Sci 2022; 21; 459–467
doi:10.2463/mrms.mp.2021-0010 Published Online: April 24, 2021

MAJOR PAPER

Cross-sectional Area of the Superior Petrosal Sinus is Reduced in Patients with Significant Endolymphatic Hydrops

Shinji Naganawa[1*], Rintaro Ito[1], Hisashi Kawai[1], Mariko Kawamura[1], Toshiaki Taoka[1], Tadao Yoshida[2], and Michihiko Sone[2]

Purpose: To evaluate the relationship between the size of the venous structures related to the inner ear and the degree of endolymphatic hydrops (EH).

Methods: Thirty-four patients with a suspicion of EH underwent whole brain MR imaging including the inner ear. Images were obtained pre- and post-administration, and at 4 and 24 hours after the intravenous administration of a gadolinium-based contrast agent (IV-GBCA). The cross-sectional areas (CSA) of the internal jugular vein (IJV), superior petrosal sinus (SPS), and inferior petrosal sinus (IPS) were measured on the magnetization prepared rapid acquisition of gradient echo (MPRAGE) images obtained immediately after the IV-GBCA. The grade of EH was determined on the hybrid of reversed image of positive endolymph signal and native image of positive perilymph signal (HYDROPS) images obtained at 4 hours after IV-GBCA as no, mild, and significant EH according to the previously proposed grading system for the cochlea and vestibule, respectively. The ipsilateral CSA was compared between groups with each level of EH grade. $P < 0.05$ was considered statistically significant.

Results: There were no statistically significant differences between EH grades for the CSA of the IJV or that of the IPS in either the cochlea or the vestibule. The CSA of the SPS in the groups with significant EH was significantly smaller than that in the group with no EH, for both the cochlea ($P < 0.01$) and the vestibule ($P < 0.05$). In an ROC analysis to predict significant EH, the cut-off CSA value in the SPS was 3.905 mm^2 for the cochlea (AUC: 0.8762, 95% confidence interval [CI]: 0.7952–0.9572) and 3.805 mm^2 for the vestibule (AUC: 0.7727, 95% CI: 0.6539–0.8916).

Conclusion: In the ears with significant EH in the cochlea or vestibule, the CSA of the ipsilateral SPS was smaller than in the ears without EH.

Keywords: *magnetic resonance imaging, gadolinium, endolymphatic hydrops, vein*

Introduction

Meniere's disease (MD) is a disorder of the inner ear, which causes vertigo attacks, fluctuating hearing loss, tinnitus, and aural fullness. The etiology of MD is multifactorial, and a characteristic sign of MD is endolymphatic hydrops (EH).[1] Direct visualization of EH is now possible by contrast enhanced MR imaging.[2–4] Currently, MR imaging obtained at 4 hours after intravenous administration of a single dose of gadolinium-based contrast agent (IV-SD-GBCA) is the method frequently utilized for a detailed evaluation of EH in the clinic.[5–7] The hybrid of reversed image of positive endolymph signal and native image of positive perilymph signal (HYDROPS) images and 3D-real inversion recovery (IR) images are widely used for this precise evaluation.[6,8,9]

The true etiology and pathophysiology of EH remains incompletely understood. Various mechanisms have been proposed for the potential causes of EH, i.e. blockage of the endolymphatic duct and sac, hypoproteinemia, increased vasopressin levels, genetic components, and vascular impairment.[1,10] The venous drainage of the inner ear is via the vein of the cochlear aqueduct and the cochlear vein,[11] and the veins of the vestibular aqueduct (the veins of the ampulla, and the superior, lateral and posterior canal). The venous

[1]Department of Radiology, Nagoya University Graduate School of Medicine, Nagoya, Aichi, Japan
[2]Department of Otorhinolaryngology, Nagoya University Graduate School of Medicine, Nagoya, Aichi, Japan

*Corresponding author: Department of Radiology, Nagoya University Graduate School of Medicine, 65, Tsurumaicho, Shouwa-ku, Nagoya, Aichi 466-8550, Japan. Phone: +81-52-744-2327, Fax: +81-52-744-2335, E-mail: naganawa@med.nagoya-u.ac.jp

Received: January 25, 2021 | Accepted: March 23, 2021

blood empties either directly into the inferior and superior petrosal sinus (IPS, SPS) or internal jugular vein (IJV).[12]

Chronic cerebrospinal venous insufficiency (CCSVI) is characterized by combined stenoses of the principal pathways for extracranial venous drainage, including the IJV and the azygos vein, with the development of collateral circles and insufficient drainage. CCSVI has been reported to be associated with multiple sclerosis (MS).[13] The CCSVI has also been reported as a potential pathogenetic mechanism for the development of MD. This vascular impairment significantly affects the venous drainage of the inner ear.[10,14] Interventional therapy for CCSVI has been reported to improve MD symptoms.[15,16] The CCSVI can be noninvasively diagnosed by combined transcranial and extracranial echo color Doppler, which measures five variables in various head positions indicative of CCSVI.[13]

Contrast enhanced 3D-T1-weighted images (CE-T1WI) obtained immediately after IV-SD-GBCA can assess the size of the SPS, IPS, and IJV, although the patient's body must be in a supine position. Compared to the HYDROPS or 3D-real IR images obtained at 4 hours after IV-SD-GBCA for the visualization of EH, CE-T1WI can be obtained in a greater population because there is no need for a long 4-hour wait time or sophisticated pulse sequences.

The purpose of this study was to evaluate if the size of the SPS, IPS, and IJV correlates with the degree of EH and to evaluate if the size of these venous structures could predict the presence of EH.

Materials and Methods

Patients

The subjects were 34 patients suspected of EH (16 women and 18 men, age: 23–80, median age: 50.5). In all cases, the estimated glomerular filtration rate was 50 mL/min/1.73 m^2 or greater. There were no cases with brain tumors or large cerebral infarctions.

MR imaging

The images were obtained pre- and post-administration, and at 4 and 24 hours after the intravenous administration of a single dose (0.1 mmol/kg) of macrocyclic GBCA (gadobutrol; Bayer Yakuhin, Osaka, Japan) (IV-SD-GBCA). Images at multiple time points were obtained to rule out tumor and vascular lesions and to assess the size of endolymphatic space, as well as the permeability of the blood-labyrinthine and blood-CSF barriers. A 3T MR scanner (MAGNETOM Skyra; Siemens Healthcare, Erlangen, Germany) with a 32-channel head coil was used.

The detailed MR parameters for the magnetization prepared rapid acquisition of gradient echo (MPRAGE),[17–19] positive perilymph image (PPI), positive endolymph image (PEI),[20,21] and 3D-real IR image[5,6,22] are shown in Table 1. The PPI is based on a heavily T2-weighted fluid attenuated inversion recovery using 3D-sampling perfection sampling perfection with application-optimized contrasts using different flip angle evolutions (SPACE) sequence. The ethical committee of our institution approved this study. Written informed consent was obtained from all patients.

Grading of EH

The presence of EH was assessed by an experienced radiologist as none, mild, and significant, using the HYDROPS images (i.e. the subtraction of the PEI from the PPI) and the 3D-real IR images obtained at 4 hours after IV-SD-GBCA according to the Nakashima grade[23] for the left and right cochlea and the vestibule, respectively. As previously reported, the Nakashima grade of the vestibule was determined on the lowest axial slice in which more than 2/3 of the lateral semicircular canal was visible.[21] For EH grading, HYDROPS images at 4 hours after IV-SD-GBCA were utilized; however, the 3D-real IR images at 4 hours after IV-SD-GBCA were referenced, if there was a mis-registration artifact on the HYDROPS images. The diagnosis of the degree of EH was already recorded in the electronic medical record of our hospital at least 6 months prior to the present study.

Measurement of the vein cross-sectional areas

The cross-sectional areas (CSA) of the IJV, SPS, and IPS were measured on MPRAGE images obtained immediately after IV-SD-GBCA. The display window width and level were set as 1000/500. On a picture archiving and communication systems (PACS) viewer (RapideyeCore; Canon Medical Systems, Tochigi, Japan), the MPRAGE images were displayed. Using the interactive multiplanar reformation (MPR) function, the CSA (mm^2) was manually measured for the right and left IJV, SPS, and IPS, respectively.

Instruction for CSA measurement in each vein is as follows:

1. For measurement of IJV, display the axial section crossing the lower edge of the anterior arch of the atlas (C1) while referring to the midsagittal section using the MPR function. Then, contour the right and left IJV using the free ROI function. Measure the CSA of the right and left IJV separately.
2. For measurement of SPS, display the axial image containing the SPS. Set an oblique coronal section perpendicular to the right SPS. Then, scroll in the oblique coronal plane and find the vertical portion of the ipsilateral facial nerve. On this oblique coronal section, measure the CSA of the SPS using the free ROI function. Note that the dura contacting the SPS should not be included in the ROI. The left side should be measured in a similar way.
3. For measurement of IPS, scroll the axial image to the level of the inferior edge of the pons, referring to the midsagittal section. Then, scroll the coronal image to the cross point of the dorsal edge of the Clivus and the

Table 1 Pulse sequence parameters

Parameter	MPRAGE	PPI and PEI	3D-real IR
Sequence type	3D Gradient echo	SPACE with inversion pulse	SPACE with inversion pulse
Slab orientation	sagittal	axial	axial
Repetition time (ms)	1570 (IR-IR), 6.7 (α-α)	9000	15130
Echo time (ms)	2.22	544	549
Inversion time (ms)	800	PPI: 2250 / PEI: 2050	2700
Fat suppression	NA	CHESS	CHESS
Flip angle (degree)	15	90/constant 120	90/constant 145
Section thickness/gap (mm)	1.0/0.0	1.0/0.0	1.0/0.0
Pixel size (mm)	1.0 × 1.0	0.5 × 0.5	0.5 × 0.5
Number of slices	256	104	256
Echo train length	1	173	256
FOV (mm)	230 × 256	165 × 196	165 × 196
Matrix size	232 × 256	324 × 384	324 × 384
Parallel imaging/Accel. factor	GRAPPA/2	GRAPPA/2	GRAPPA/3
Band width (Hz/Px)	200	434	434
Number of excitations	1	2	1
Scan time (min)	3	7 for each	11

3D-real IR, 3D real inversion recovery with phase sensitive reconstruction; α-α, time between α pulses; CHESS, chemical shift selective; GRAPPA, generalized autocalibrating partially parallel acquisition; IR-IR, time between inversion pulses; MPRAGE, magnetization prepared rapid gradient echo; NA, not applicable; PEI, positive endolymph image; PPI, positive perilymph image; SPACE, sampling perfection with application-optimized contrasts using different flip angle evolutions.

axial image to the level of the inferior edge of the pons. On this coronal section, measure the CSA of the right and left IPS separately. Note that the dura contacting the IPS should not be included in the ROI. Although this coronal section might not be completely perpendicular to IPS, this coronal section was designated to provide high reproducibility.

Two experienced neuroradiologists (S.N. and H.K. with 33 and 23 years of experience, respectively) independently measured the CSA of the veins after attending the training session together, using the two cases of image data not included in the present study. The intraclass correlation coefficients (ICC [2,1]) for the agreement of the measured CSA between the two radiologists were calculated. The values by the two radiologists were averaged and used for the subsequent analysis. Examples for the ROI placement are shown in Fig. 1.

Statistical analysis

The ICC (2, 1) was calculated to evaluate the interobserver reliability.

The CSA of the ipsilateral venous structures was compared between the ears with no, mild, and significant EH for the cochlea and vestibular using analysis of variance (ANOVA) with Bonferroni correction for multiple comparisons. For the CSA of the venous structure with a significant difference between the EH grades, a receiver operating characteristic (ROC) analysis was performed and the area under the curve (AUC) was measured. The cut-off value of the CSA for prediction of significant EH was determined by maximization of the Youden index (sensitivity + specificity − 1).

We used SPSS Statistics software version 27.0.0. 64bit (IBM, Chicago, IL USA) for the ICC (2, 1) and ANOVA statistical analyses. A value of 5% was adopted as the significance level for statistical testing. The software R (version 3.3.2; R Foundation for Statistical Computing, Vienna, Austria, https://www.R-project.org/) was used for the ROC analyses.

Results

Distribution of EH grades in all 68 ears for cochlea was 19 ears with no EH, 20 ears with mild EH, and 29 ears with

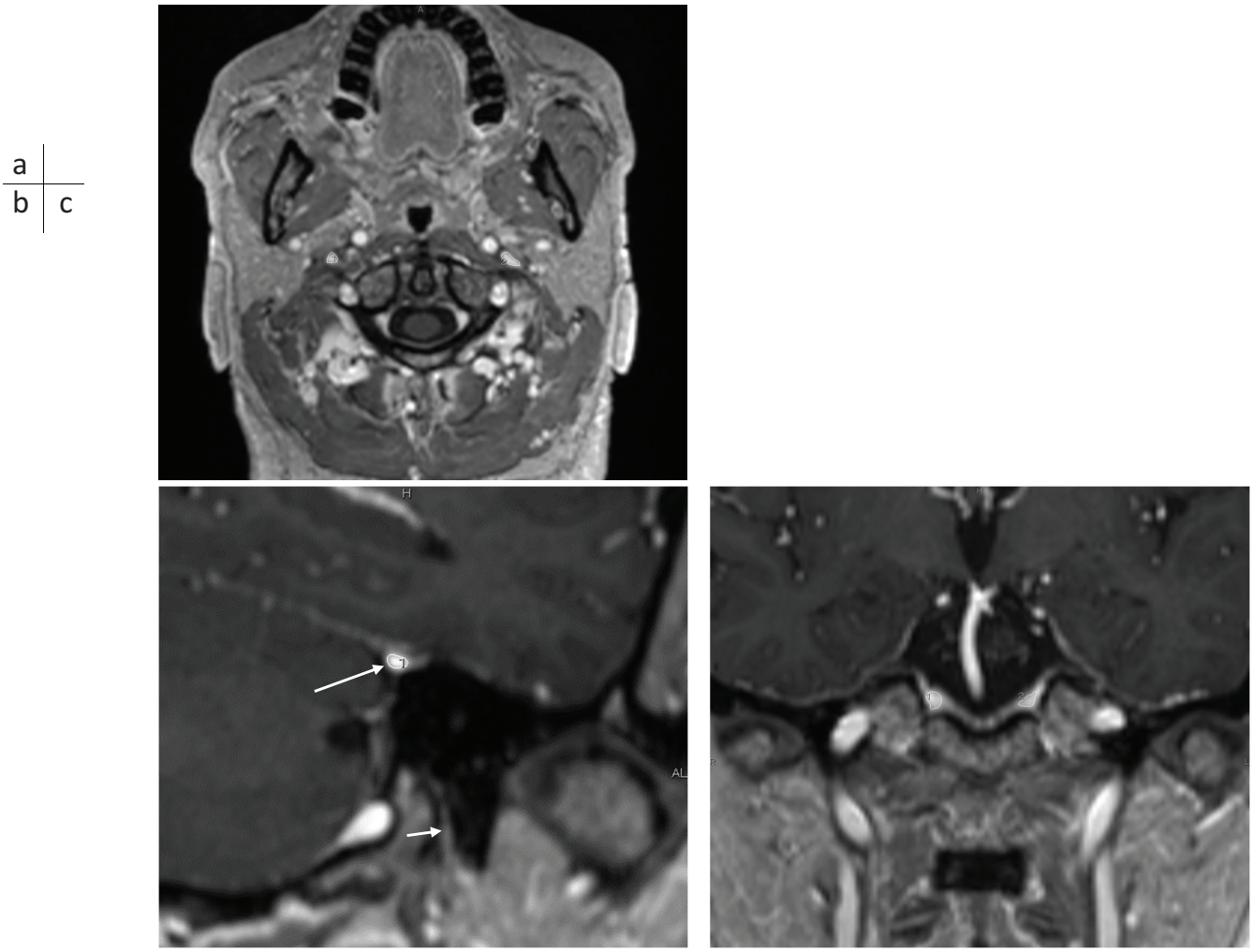

Fig. 1 Examples of the ROI placement on contrast enhanced MPRAGE images. (**a**) On an axial section at the level of the inferior edge of the anterior arch of the atlas, the internal jugular vein of each side was manually contoured (ROI #1 and #2). (**b**) On an oblique coronal section, perpendicular to the SPS (arrow) at the level of the vertical portion of the facial nerve (short arrow), the SPS was contoured (ROI #1). (**c**) On a coronal section as described in the Methods, the IPS of each side was manually contoured (ROI #1 and #2). IPS, inferior petrosal sinus; MPRAGE, magnetization prepared rapid acquisition of gradient echo; SPS, superior petrosal sinus.

significant EH, while that for vestibule was 50 ears with no EH, 7 ears with mild EH, and 11 ears with significant EH.

The ICCs (2, 1) between two observers were quite high at 0.997 (95% confidence interval; 0.994–0.999) for IJV, 0.988 (0.971–0.994) for SPS, and 0.978 (0.737–0.993) for IPS.

The average ($\pm$ standard deviation) CSAs (mm^2) were 21.5 $\pm$ 15.3 for IJV, 4.0 $\pm$ 1.9 for SPS, and 8.1 $\pm$ 4.3 for IPS. The box-and-whisker plots of each EH group for IJV, SPS, and IPS are shown in Figs. 2a-f. There were two sides of hypoplastic IJV. For these hypoplastic IJVs, CSA was set as 0 by both observers. There was a hypoplastic SPS. For this SPS, CSA was set as 0 by both observers.

For the CSA of IJV and IPS, there was no significant differences between the ears with different EH grades.

There was a significant difference of the mean CSA of the SPS between the ears with no cochlear EH and significant cochlear EH ($P < 0.01$) and between the ears with mild cochlear EH and significant cochlear EH ($P < 0.01$).

There was a significant difference of the mean CSA of the SPS between the ears with no vestibular EH and significant vestibular EH ($P < 0.05$; $P = 0.020$)

The ROC curve for predicting cochlear significant EH by the CSA of the SPS is shown in Fig. 3a. The AUC was 0.8762 (95% CI: 0.7952–0.9572). The cut-off value of the CSA for the SPS was 3.905 mm^2 (specificity of 0.828, sensitivity of 0.795, positive predictive value of 0.861, and negative predictive value of 0.750).

The ROC curve for predicting significant EH in the vestibule by the CSA of the SPS is shown in Fig. 3b. The AUC was 0.7727 (95% CI: 0.6539–0.8916). The cut-off value of the CSA for the SPS was 3.805 mm^2 (specificity of 0.909,

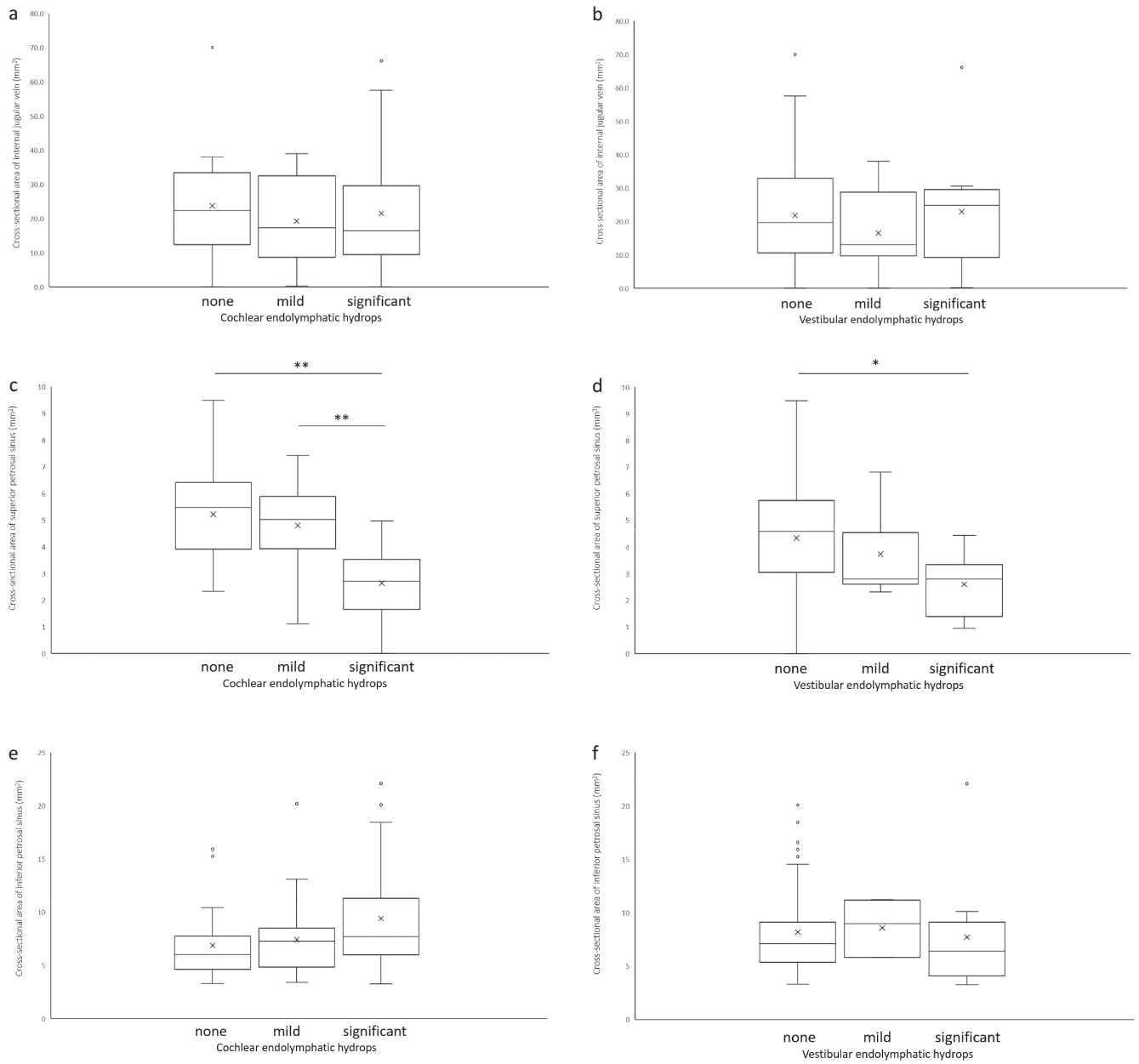

Fig. 2 (**a**) A box-and-whisker plot of the cross-sectional area of the IJV of the group without cochlear EH, the mild EH group, and the significant EH group. The lower side of the rectangle is the first quartile (25th percentile value) and the upper side is the 75th percentile value. The thick horizontal line in the rectangle is the median. The horizontal line under the whisker indicates the 10th percentile value, and the horizontal line above the whisker indicates the 90th percentile value. There is an overlap between the three groups and there were no significant differences between the groups. (**b**) A box-and-whisker plot of the cross-sectional area of the IJV in the group without vestibular EH, the mild EH group, and the significant EH group. There is an overlap between the three groups and there were no significant differences between the groups. (**c**) A box-and-whisker plot of the cross-sectional area of the SPS of the group without cochlear EH, the mild EH group, and the significant EH group. There were some overlaps between the three groups; however, there were significant differences between the groups (**$P < 0.01$). (**d**) A box-and-whisker plot of the cross-sectional area of the SPS of the group without vestibular EH, the mild EH group, and the significant EH group. There were some overlaps between the three groups; however, there were significant differences between the groups (*$P < 0.05$). (**e**) A box-and-whisker plot of the cross-sectional area of the IPS of the group without cochlear EH, the mild EH group, and the significant EH group. There was an overlap between the three groups, and there was no significant difference between the groups. (**f**) A box-and-whisker plot of the cross-sectional area of the IPS of the group without vestibular EH, the mild EH group, and the significant EH group. There was an overlap between the three groups, and there was no significant difference between the groups. EH, endolymphatic hydrops; IJV, internal jugular vein; IPS, inferior petrosal sinus; SPS, superior petrosal sinus.

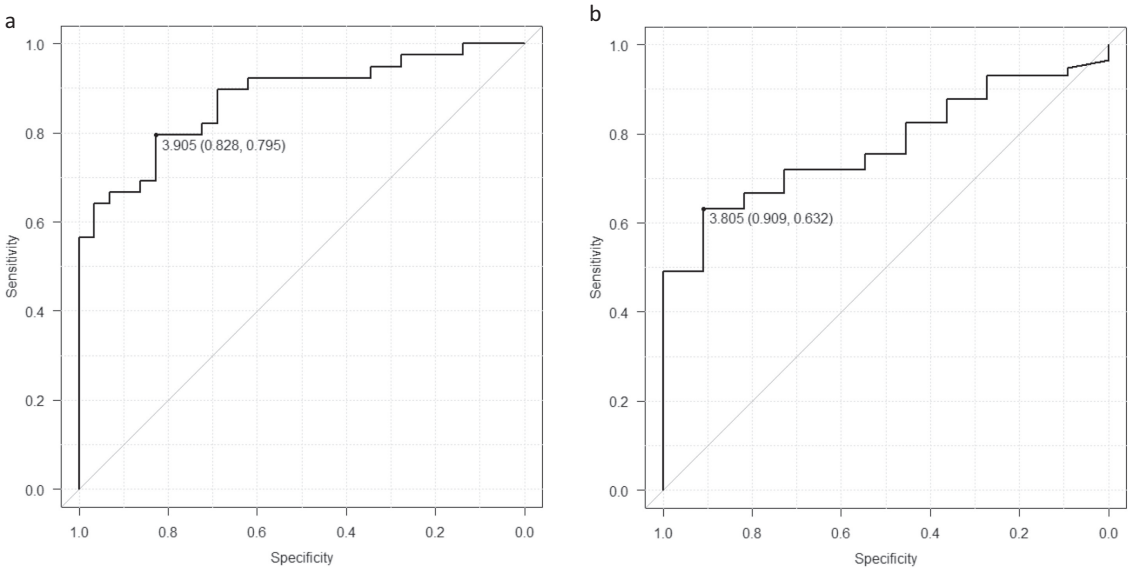

Fig. 3 (**a**) ROC curve for significant cochlear endolymphatic hydrops by the cross-sectional area of the superior petrosal sinus. The AUC was 0.8762 with a 95% CI: 0.7952–0.9572. The cut-off value of 3.905 mm^2 (Youden index) provided a specificity of 0.828 and a sensitivity of 0.795. (**b**) The ROC curve for the group with significant vestibular endolymphatic hydrops by the cross-sectional area of the superior petrosal sinus. The AUC was 0.7727 with a 95% CI: 0.6539–0.8916. The cut-off value of 3.805 mm^2 (Youden index) provided a specificity of 0.909 and a sensitivity of 0.623. AUC, area under the curve; CI, confidence interval; ROC, receiver operating characteristic.

sensitivity of 0.632, positive predictive value of 0.973, and negative predictive value of 0.323).

Images from representative patients are shown in Figs. 4 and 5.

Discussion

There is increasing interest in the relationship between venous blood flow and EH.[14] In order to improve CCSVI, percutaneous transluminal angioplasty of the jugular vein has been performed and was effective in 80% of patients.[15] MD, along with glaucoma, is a neurodegenerative disease of the sensory organs.[24] Neurofluidic dynamics have been proposed as an important factor in the pathogenesis of neurodegenerative diseases.[25,26] Venous and interstitial fluid flows are also important components of the glymphatic system, which is the waste clearance mechanism of the central nervous system.[25,27,28]

In the present study, an evaluation of the venous CSA in a static state showed no significant association between EH grades in the cochlea or vestibule for the IJV or IPS. However, the SPS was associated significantly with EH grade. The CSA of the SPS was smaller in ears with significant EH than those without EH in both the cochlea and the vestibule. However, in both the cochlea and the vestibule, there is an overlap in the CSA of the SPS between each EH grade group, making it difficult to use the CSA of the SPS to differentiate individual diagnoses. In the ROC analysis of the cochlea, the AUC for predicting significant EH was 0.8762, and the threshold value was 3.905 mm^2. In the vestibule, the AUC for predicting significant EH was 0.7727, with a threshold of 3.805 mm^2. The negative predictive value was 0.750 for the cochlear EH but was only 0.323 for the vestibular EH.

It cannot be determined from the present results whether the size of the SPS directly reflects the effect of congestion in the inner ear on venous blood drainage, or if it reflects an indirect relationship between the size of the SPS and the development of an unknown specific region of the temporal bone associated with EH. The IPS should also influence the inner ear blood flow drainage, but in the present study, there was no relationship between the CSA of the IPS and the degree of EH. In other words, the relationship between the CSA of the SPS and the degree of EH may be showing an indirect effect by the development of a specific region of the temporal bone rather than a direct effect of inner ear blood flow congestion.

To further investigate the results of this study, it is necessary to investigate the distribution of the CSA of the SPS in a healthy cohort in the future. It is also clinically important to investigate whether there is an association between the onset of MD and the fluctuation of the SPS CSA in a prospective study. In addition, a search for temporal bone regions, which are associated with the SPS CSA, may be necessary.

Some other morphological features, which may be associated with MD, have already been reported as described below. Visibility of the vestibular aqueduct on CT was reported to be correlated with the presence of EH on the MR images obtained at 4 hours after the GBCA administration.[29] It was reported that the diameter of the medial side of the cochlear aqueduct is narrow in patients with MD.[30] There has been a debate about the significance of high jugular bulbs in the development of EH. In one report, a high jugular bulb was

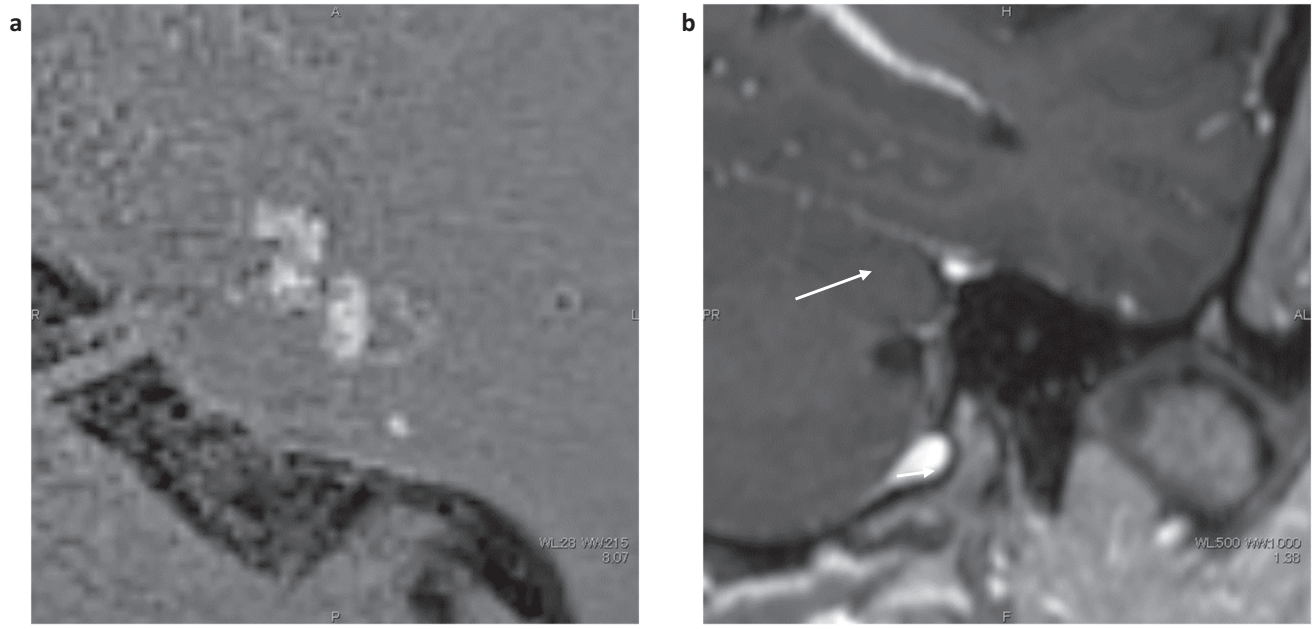

Fig. 4 A male patient in his 50s. (**a**) On the HYDROPS image, there is no endolymphatic hydrops in the left inner ear for either the cochlea or the vestibule. (**b**) An oblique coronal MPRAGE image obtained immediately after IV-GBCA, perpendicular to the superior petrosal sinus. A well-developed superior petrosal sinus is visualized (arrow). The vertical portion of the facial nerve is seen (short arrow). HYDROPS, hybrid of reversed image of positive endolymph signal and native image of positive perilymph signal; IV-GBCA, intravenous administration of a gadolinium-based contrast agent; MPRAGE, magnetization prepared rapid acquisition of gradient echo.

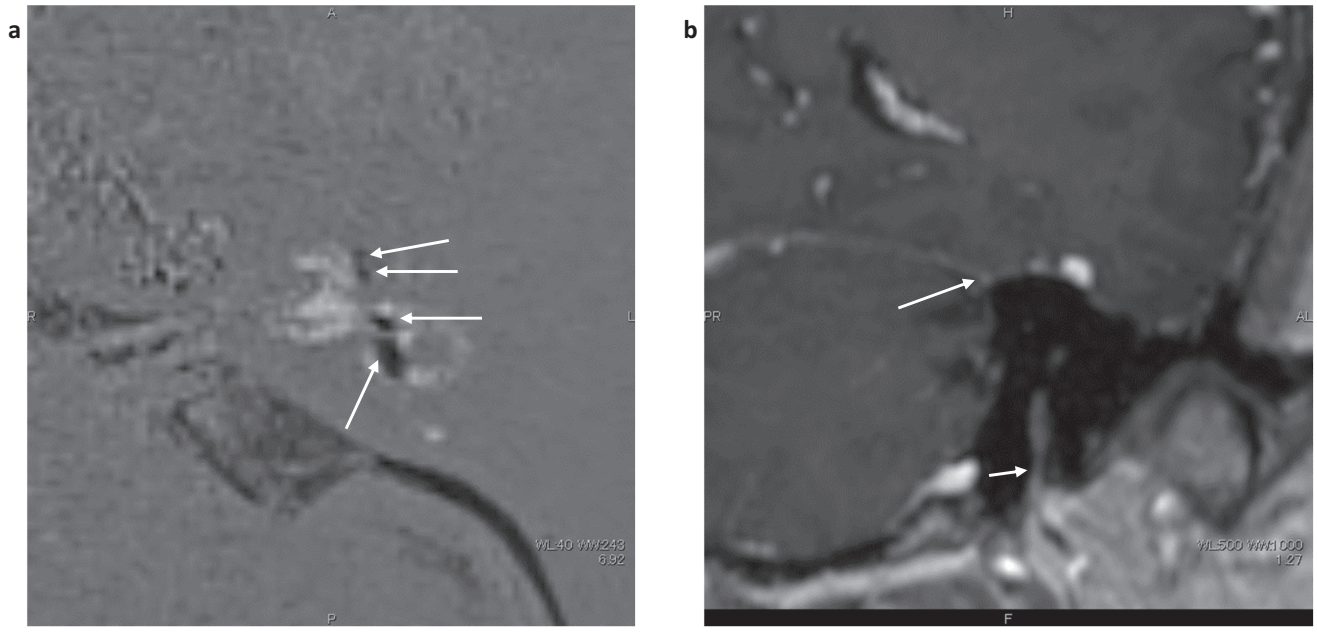

Fig. 5 A male patient in his 50s. (**a**) There is significant endolymphatic hydrops in the left inner ear in both the cochlea and the vestibule on the HYDROPS image (arrows). (**b**) An oblique coronal MPRAGE image obtained immediately after IV-GBCA, perpendicular to the superior petrosal sinus. A poorly developed superior petrosal sinus is visualized (arrow). The vertical portion of the facial nerve is seen (short arrow). HYDROPS, hybrid of reversed image of positive endolymph signal and native image of positive perilymph signal; IV-GBCA, intravenous administration of a gadolinium-based contrast agent; MPRAGE, magnetization prepared rapid acquisition of gradient echo.

reported to be related to the development of EH. It was suggested that a jugular bulb reaching above the inferior margin of the internal auditory canal could obstruct the vestibular aqueduct, resulting in EH.[31] Alternatively, it was reported that a high jugular bulb is not the cause of EH in patients with MD.[32] Both studies used GBCA-enhanced MRI as the reference for EH. It was also reported that poor development of the air cells around the vestibular aqueduct is not associated with EH.[32]

Superior semicircular canal dehiscence syndrome and large vestibular aqueduct syndrome (LVAS) are reported to be related to a high incidence of EH.[33,34] Pathologic third window lesions, such as superior semicircular canal dehiscence syndrome or LVAS, cause several auditory and vestibular symptoms, which might affect the perilymphatic pressure and induce EH. There was a case report indicating that a deep groove in the SPS might have caused superior semicircular canal dehiscence syndrome and possible EH. The symptoms resolved after plugging the dehiscence through a middle cranial fossa approach.[35] Another report showed that stenting of the SPS significantly decreased the symptoms of superior semicircular canal dehiscence by the SPS.[36]

The CSA of the SPS is relatively easy to examine compared to the degree of EH. If we can efficiently predict the future development of EH in patients from small SPS CSA values, we may be able to prevent the onset of MD by early lifestyle changes.

The limitations of the present study are as follows. The number of cases was small in this study. Although the agreement between examiners was good, manual measurements of the CSA of the venous structure could be performed automatically in the future. Quantification of EH might be valuable to further elucidate the relationship between EH and SPS CSA.

The CSA of the venous structures might be affected by body position and respiratory status, but in the present study, it was only evaluated in a static supine position. The precise flow measurement, including the collateral venous flow, might be necessary to elucidate the relationship between venous congestion and EH; however, we employed static measurement of CSA in the present study. We focused on searching for a surrogate imaging biomarker of EH that could be easily obtained. The static CSA of SPS is relatively easy to obtain and might be a candidate for a surrogate imaging biomarker of EH. As mentioned above, the mechanism of the relationship between the degrees of venous development and EH remains unknown. Since MD progresses over a long period of time, it would be interesting to see if the CSA of the SPS is altered between the early and late stages of MD, but further investigation with a larger number of patients over a longer period is necessary.

Conclusion

The results of this preliminary study showed that there was an association between the degree of EH and the CSA of the SPS, but not that of the IPS or IJV. Further studies are needed to establish the pathophysiological and clinical significance of the present results.

Funding

This study was supported in part by Grants-in-Aid for scientific research from the Japanese Society for the Promotion of Science (JSPS KAKENHI, numbers 17H04259, 18K19510) to S.N.

Conflicts of Interest

Toshiaki Taoka and Rintaro Ito are the professors in the Department of Innovative Biomedical Visualization (iBMV), which is financially supported by CANON MEDICAL SYSTEMS CORPORATION. All other authors declare that they have no conflicts of interest regarding this manuscript.

References

1. Nakashima T, Pyykkö I, Arroll MA, et al. Meniere's disease. Nat Rev Dis Primers 2016; 2:16028.
2. Nakashima T, Naganawa S, Sugiura M, et al. Visualization of endolymphatic hydrops in patients with Meniere's disease. Laryngoscope 2007; 117:415-420.
3. Naganawa S, Kawai H, Sone M, et al. Increased sensitivity to low concentration gadolinium contrast by optimized heavily T2-weighted 3D-FLAIR to visualize endolymphatic space. Magn Reson Med Sci 2010; 9:73-80.
4. Naganawa S, Yamazaki M, Kawai H, et al. Imaging of Ménière's disease after intravenous administration of single-dose gadodiamide: utility of subtraction images with different inversion time. Magn Reson Med Sci 2012; 11:213-219.
5. Naganawa S, Kawai H, Taoka T, et al. Improved 3D-real inversion recovery: a robust imaging technique for endolymphatic hydrops after intravenous administration of gadolinium. Magn Reson Med Sci 2019; 18:105-108.
6. Ohashi T, Naganawa S, Takeuchi A, et al. Quantification of endolymphatic space volume after intravenous administration of a single dose of gadolinium-based contrast agent: 3D-real inversion recovery versus HYDROPS-Mi2. Magn Reson Med Sci 2020; 19:119-124.
7. Naganawa S, Nakashima T. Visualization of endolymphatic hydrops with MR imaging in patients with Ménière's disease and related pathologies: current status of its methods and clinical significance. Jpn J Radiol 2014; 32:191-204.
8. Naganawa S, Yamazaki M, Kawai H, et al. Imaging of Ménière's disease by subtraction of MR cisternography from positive perilymph image. Magn Reson Med Sci 2012; 11:303-309.
9. Liu IY, Sepahdari AR, Ishiyama G, et al. High resolution MRI shows presence of endolymphatic hydrops in patients still symptomatic after endolymphatic shunt surgery. Otol Neurotol 2016; 37:1128-1130.
10. Filipo R, Ciciarello F, Attanasio G, et al. Chronic cerebrospinal venous insufficiency in patients with Ménière's disease. Eur Arch Otorhinolaryngol 2015; 272:77-82.

11. Axelsson A. Comparative anatomy of cochlear blood vessels. Am J Otolaryngol 1988; 9:278-290.
12. Mazzoni A. The vascular anatomy of the vestibular labyrinth in man. Acta Otolaryngol Suppl 1990; 472:1-83.
13. Zamboni P, Galeotti R, Menegatti E, et al. A prospective open-label study of endovascular treatment of chronic cerebrospinal venous insufficiency. J Vasc Surg 2009; 50:1348-1358.e1-3.
14. Di Berardino F, Alpini DC, Bavera PM, et al. Chronic cerebrospinal venous insufficiency in Ménière disease. Phlebology 2015; 30:274-279.
15. Bruno A, Napolitano M, Califano L, et al. The Prevalence of chronic cerebrospinal venous insufficiency in meniere disease: 24-month follow-up after angioplasty. J Vasc Interv Radiol 2017; 28:388-391.
16. Attanasio G, Califano L, Bruno A, et al. Chronic cerebrospinal venous insufficiency and menière's disease: Interventional versus medical therapy. Laryngoscope 2020; 130:2040-2046.
17. de Lange EE, Urbanski SR, Mugler JP, et al. Magnetization-prepared rapid gradient echo (MP-RAGE) magnetic resonance imaging of Morgagni's hernia. Eur J Radiol 1990; 11:196-199.
18. Runge VM, Kirsch JE, Thomas GS, et al. Clinical comparison of three-dimensional MP-RAGE and FLASH techniques for MR imaging of the head. J Magn Reson Imaging 1991; 1:493-500.
19. Ikushima I, Korogi Y, Kitajima M, et al. Evaluation of drainage patterns of the major anastomotic veins on the lateral surface of the cerebrum using three-dimensional contrast-enhanced MP-RAGE sequence. Eur J Radiol 2006; 58:96-101.
20. Naganawa S, Yamazaki M, Kawai H, et al. Imaging of Ménière's disease after intravenous administration of single-dose gadodiamide: utility of subtraction images with different inversion time. Magn Reson Med Sci 2012; 11:213-219.
21. Naganawa S, Suzuki K, Nakamichi R, et al. Semi-quantification of endolymphatic size on MR imaging after intravenous injection of single-dose gadodiamide: comparison between two types of processing strategies. Magn Reson Med Sci 2013; 12:261-269.
22. Naganawa S, Nakane T, Kawai H, et al. Age dependence of gadolinium leakage from the cortical veins into the cerebrospinal fluid assessed with whole brain 3D-real inversion recovery MR imaging. Magn Reson Med Sci 2019; 18:163-169.
23. Nakashima T, Naganawa S, Pyykko I, et al. Grading of endolymphatic hydrops using magnetic resonance imaging. Acta Otolaryngol Suppl 2009; 560:5-8.
24. Nakashima T, Sone M, Teranishi M, et al. A perspective from magnetic resonance imaging findings of the inner ear: Relationships among cerebrospinal, ocular and inner ear fluids. Auris Nasus Larynx 2012; 39:345-355.
25. Taoka T, Naganawa S. Neurofluid dynamics and the glymphatic system: a neuroimaging perspective. Korean J Radiol 2020; 21:1199-1209.
26. Agarwal N, Contarino C, Toro E. Neurofluids: A holistic approach to their physiology, interactive dynamics and clinical implications for neurological diseases. Veins and Lymphatics 2019; 8:49-58.
27. Naganawa S, Taoka T. The glymphatic system: a review of the challenges in visualizing its structure and function with MR imaging. Magn Reson Med Sci 2020 Nov 27. doi: 10.2463/mrms.rev.2020-0122. [Epub ahead of print]
28. Taoka T, Naganawa S. Imaging for central nervous system (CNS) interstitial fluidopathy: disorders with impaired interstitial fluid dynamics. Jpn J Radiol 2021; 39:1-14.
29. Mainnemarre J, Hautefort C, Toupet M, et al. The vestibular aqueduct ossification on temporal bone CT: an old sign revisited to rule out the presence of endolymphatic hydrops in Menière's disease patients. Eur Radiol 2020; 30:6331-6338.
30. Song CI, Kang WS, Lee JH, et al. Diameter of the medial side of the cochlear aqueduct is narrower in Meniere's disease: a radiologic analysis. J Int Adv Otol 2016; 12:156-160.
31. Hu J, Peng A, Deng K, et al. Value of CT and three-dimensional reconstruction revealing specific radiological signs for screening causative high jugular bulb in patients with Meniere's disease. BMC Med Imaging 2020; 20:103.
32. Oya R, Imai T, Sato T, et al. A high jugular bulb and poor development of perivestibular aqueductal air cells are not the cause of endolymphatic hydrops in patients with Ménière's disease. Auris Nasus Larynx 2018; 45:693-701.
33. Sone M, Yoshida T, Morimoto K, et al. Endolymphatic hydrops in superior canal dehiscence and large vestibular aqueduct syndromes. Laryngoscope 2016; 126:1446-1450.
34. Ray A, Hautefort C, Guichard JP, et al. MRI contribution for the detection of endolymphatic hydrops in patients with superior canal dehiscence syndrome. Eur Arch Otorhinolaryngol 2020 Aug 14. doi: 10.1007/s00405-020-06282-3. [Epub ahead of print]
35. Koo JW, Hong SK, Kim DK, et al. Superior semicircular canal dehiscence syndrome by the superior petrosal sinus. J Neurol Neurosurg Psychiatry 2010; 81:465-467.
36. Ionescu EC, Coudert A, Reynard P, et al. Stenting the superior petrosal sinus in a patient with symptomatic superior semicircular canal dehiscence. Front Neurol 2018; 9:689.